

Powder metallurgy of Al-based metal matrix composites reinforced with β -Al₃Mg₂ intermetallic particles: Analysis and modeling of mechanical properties

S. Scudino^{a,*}, G. Liu^{a,b}, M. Sakaliyska^a, K.B. Surreddi^a, J. Eckert^{a,c}

^a IFW Dresden, Institut für Komplexe Materialien, Postfach 27 01 16, D-01171 Dresden, Germany

^b State Key Laboratory for Mechanical Behavior of Materials, School of Materials Science and Engineering, Xi'an Jiaotong University, Xi'an 710049, China

^c TU Dresden, Institut für Werkstoffwissenschaft, D-01062 Dresden, Germany

Received 7 April 2009; received in revised form 7 June 2009; accepted 15 June 2009

Available online 17 July 2009

Abstract

In order to analyze the effectiveness of complex metallic alloys as reinforcing agents in metal matrix composites, Al-based composites were synthesized by hot extrusion of elemental Al blended with different amounts of β -Al₃Mg₂ complex intermetallic particles. The work focuses on two specific aspects: evaluation of the mechanical properties through room temperature compression tests and modeling of the resulting properties. The β -Al₃Mg₂ reinforcement remarkably improves the mechanical properties of pure Al. In particular, the composites with 20 and 40 vol.% reinforcement display yield and compressive strengths exceeding that of pure Al by a factor of 2–3, while retaining appreciable plastic deformation ranging between 45% and 15%. Moreover, the addition of low-density β -Al₃Mg₂ particles significantly increases the specific strength of the composites. Finally, modeling of the mechanical properties reveals that the matrix ligament size plays a dominant role for affecting the properties of the composites.

© 2009 Acta Materialia Inc. Published by Elsevier Ltd. All rights reserved.

Keywords: Powder consolidation; Metal matrix composites (MMC); Complex metallic alloys (CMA); Mechanical properties; Micromechanical modeling

1. Introduction

As a result of the increasingly severe requirements for limiting fuel consumption and carbon dioxide emission, there is a growing trend to reduce the structural weight of vehicles in the transport sector [1,2]. Most of the improvements have been achieved in the automotive sector, with the substitution of aluminum alloys for steel or cast iron [3]. However, the intense use of aluminum is hindered by the high cost of primary aluminum as compared to steel and added fabrication costs of aluminum components [3]. Therefore, radical advances in terms of the specific properties are needed to make aluminum a cost-effective alternative to steel.

Among the advanced engineering materials for transport applications, Al-based metal matrix composites (MMCs) show the largest potential to reach this goal and to develop novel lightweight high-performance materials due to their remarkable properties, including low density, high strength and good fatigue and wear resistance [4–8]. In addition, MMCs offer the possibility to tailor their properties to meet specific requirements, which renders this type of material quite unique in comparison to conventional unreinforced materials [4–8].

The family of the discontinuously reinforced MMCs (e.g. particulate-reinforced composites) is particularly attractive due to their easier fabrication routes, lower costs and nearly isotropic properties [4] compared to the continuously reinforced MMCs. Furthermore, an additional advantage of the discontinuously reinforced over the continuously reinforced MMCs is that most existing process-

* Corresponding author. Tel.: +49 351 4659 838; fax: +49 351 4659 452.
E-mail address: s.scudino@ifw-dresden.de (S. Scudino).

ing techniques can be used for fabrication and finishing of the composites, including hot rolling, hot forging, hot extrusion and machining [5,8].

Discontinuously reinforced MMCs can be successfully prepared by powder metallurgy (P/M) [9–17]. The main advantage of P/M over other methods, such as liquid phase processing, is the microstructure control of the phases (e.g. volume fraction, size and morphology of matrix and reinforcement) that is virtually absent from the liquid phase route [18]. In addition, the relatively low processing temperature of P/M may avoid undesired interfacial reactions between matrix and reinforcement [18,19].

Different types of materials, ranging from the typical ceramic reinforcements, such as Al_2O_3 and SiC [5,9,10], to more unconventional reinforcements, such as metallic glasses [11–14] and quasicrystals [15–17], have been successfully used as reinforcements in MMCs. Other possible candidates as reinforcing agents in MMCs are complex metallic alloys (CMAs), intermetallic compounds with giant unit cells, comprising up to more than a thousand atoms per unit cell [20]. CMAs have recently attracted much attention ranging from scientific curiosity about their complex structure, physical and mechanical properties to technological aspects of preparation and potential applications [20–29]. In particular, CMAs display several attractive properties for reinforcement applications, such as high strength to weight ratio, good oxidation resistance and high-temperature strength [21,27–29].

Among the different CMAs, the $\beta\text{-Al}_3\text{Mg}_2$ phase (1168 atoms per unit cell) [21] has been extensively investigated with particular attention to its structure as well as to its physical and mechanical properties [21–23,28] and, therefore, it represents the ideal complex intermetallic compound to analyze the effectiveness of CMAs as reinforcing agents in metal matrix composites. In addition, the $\beta\text{-Al}_3\text{Mg}_2$ phase displays interesting properties, such as low density (about 2.25 g cm^{-3} [21]) and high-temperature strength ($\sim 300 \text{ MPa}$ at 573 K [28]), which further makes this material an attractive candidate as reinforcement in MMCs.

Accordingly, in this work, Al-based metal matrix composites containing high-strength $\beta\text{-Al}_3\text{Mg}_2$ CMA particles have been produced by powder metallurgy. To test the effect of the $\beta\text{-Al}_3\text{Mg}_2$ phase on the properties of the composites, the work was focused on two specific aspects: evaluation of the mechanical properties through room temperature compression tests and modeling of the resulting properties. The results reveal that the properties can be successfully predicted by taking into account the matrix ligament size effect.

2. Experimental

Powders with nominal composition $\text{Al}_{60}\text{Mg}_{40}$ (corresponding to the equilibrium phase $\beta\text{-Al}_3\text{Mg}_2$ [21]) were produced by mechanical alloying of elemental powder mixtures (purity $>99.9\text{wt.}\%$) using a Retsch PM400 planetary

ball mill and hardened steel balls and vials. The powders were milled for 100 h with a ball-to-powder mass ratio (BPR) of 13:1 and a milling intensity of 150 rpm. To avoid or minimize possible atmosphere contamination during milling, vial charging and any subsequent sample handling was carried out in a glove box under purified argon atmosphere (less than 1 ppm O_2 and H_2O). Al-based metal matrix composites consisting of elemental Al powder blended with different amounts (20, 40, 60 and 80 vol.%) of $\beta\text{-Al}_3\text{Mg}_2$ powders were synthesized through powder metallurgy methods. Consolidation was done by uniaxial hot pressing followed by hot extrusion under argon atmosphere at 673 K and 500 MPa . The extrusion ratio was 6:1. The density of the consolidated samples was evaluated by the Archimedes principle. The phases and the microstructure were characterized by X-ray diffraction (XRD) using a Philips PW 1050 diffractometer ($\text{Co K}\alpha$ radiation) and by scanning electron microscopy (SEM) using a Hitachi TM-1000 tabletop microscope. The matrix ligament size (λ) was measured by superposing random lines on the SEM micrographs of the composites and its value was determined from the number of matrix region intercepts per unit length of test line, N , and the total length fell into the matrix (L) as $\lambda = L/N$ [30]. Ten random lines were superposed on each micrographs and a minimum of three micrographs was used per composite. According to the ASTM standard for compression testing [31], cylinders with a length/diameter ratio of 2.0 (8 mm length and 4 mm diameter) were prepared from the extruded samples. The specimens were tested with an INSTRON 8562 testing facility under quasistatic loading (strain rate of $8 \times 10^{-4} \text{ s}^{-1}$) at room temperature. Both ends of the specimens were polished to make them parallel to each other prior to the compression test.

3. Results and discussion

3.1. Consolidation and mechanical properties

In order to produce Al-based MMCs reinforced with CMA particles, elemental Al powder was blended with different volume fractions (V) of $\beta\text{-Al}_3\text{Mg}_2$ powder. The $\beta\text{-Al}_3\text{Mg}_2$ CMA reinforcement used in the present work was produced by MA of elemental powder mixtures. The details about preparation and characterization of the milled powder can be found in Ref. [32]. The composite powders were then consolidated by hot pressing followed by hot extrusion at 673 K . This gives rise to consolidated composites with a relative density of about 98%. For comparison purposes, a bulk specimen was produced by extrusion of pure Al powder using the same consolidation parameters as used for the MMCs.

The XRD patterns of the composites reinforced with different amounts of $\beta\text{-Al}_3\text{Mg}_2$ particles are presented in Fig. 1. All the patterns display the intense and sharp diffraction peaks due to the Al matrix along with the signals of the $\beta\text{-Al}_3\text{Mg}_2$ phase. The relative intensity of the peaks belonging to the $\beta\text{-Al}_3\text{Mg}_2$ phase remarkably increases

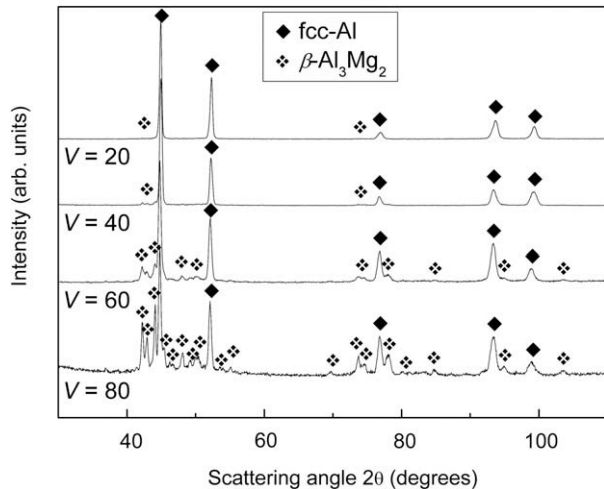


Fig. 1. XRD patterns (Co K α radiation) for the hot pressed and hot extruded composites with 20, 40, 60 and 80 vol.% of β -Al $_3$ Mg $_2$ reinforcement.

with increasing volume fraction of the reinforcement from $V = 20$, where only few and weak peaks of β -Al $_3$ Mg $_2$ are visible, to $V = 80$, where all the diffraction signals of β -Al $_3$ Mg $_2$ can be clearly observed. No additional diffraction peaks can be detected, implying that face-centered cubic (fcc) Al and β -Al $_3$ Mg $_2$ are the only phases present.

Fig. 2 shows the SEM micrographs taken from the cross-section of the consolidated composites. The images display a microstructure consisting of dark areas (the β -Al $_3$ Mg $_2$ CMA reinforcement) homogeneously dispersed in the Al matrix (the bright regions). The regions of β -Al $_3$ Mg $_2$ become more interconnected with increasing amount of

reinforcement. Only few pores are visible, further corroborating the high density of the consolidated specimens.

Fig. 3 displays the density of the composites as a function of the volume fraction of reinforcement. The density linearly decreases with increasing amount of β -Al $_3$ Mg $_2$ from about 2.7 g cm^{-3} for pure Al to 2.4 g cm^{-3} for the composite with $V = 80$. This leads to a reduction of density of about 0.1% for each vol.% of β -Al $_3$ Mg $_2$ added.

Typical room temperature uniaxial compression true stress–true strain curves of the tests under quasistatic loading for the composite materials are shown in Fig. 4 together with the curve for the extruded pure Al ($V = 0$). The addition of the CMA reinforcement is very effective for improving the mechanical properties of the Al matrix. In particular, the composites with 20 and 40 vol.% of β -Al $_3$ Mg $_2$ display a remarkable deformation behavior. The specimen with $V = 20$ exhibits a yield strength (offset = 0.2%) of about 227 MPa. After yielding the stress increases with increasing strain and the sample exhibits a pronounced work-hardening up to 485 MPa, reaching an ultimate strain of 45% before fracture occurs. With increasing the volume fraction of β -Al $_3$ Mg $_2$ to 40 vol.% the yield as well as the compressive strength (the maximum compressive stress which the material is capable of sustaining [33]) both further raise to about 342 and 530 MPa, respectively, and the strain at break is about 15%. These results indicate that the addition of the CMA reinforcement leads to composite materials with yield and compressive strengths exceeding that of pure Al by a factor of 2–3, while retaining appreciable plastic deformation. The strength of the material is further increased to 575 and 630 MPa for the samples with 60 and 80 vol.% of β -Al $_3$ Mg $_2$ phase, how-

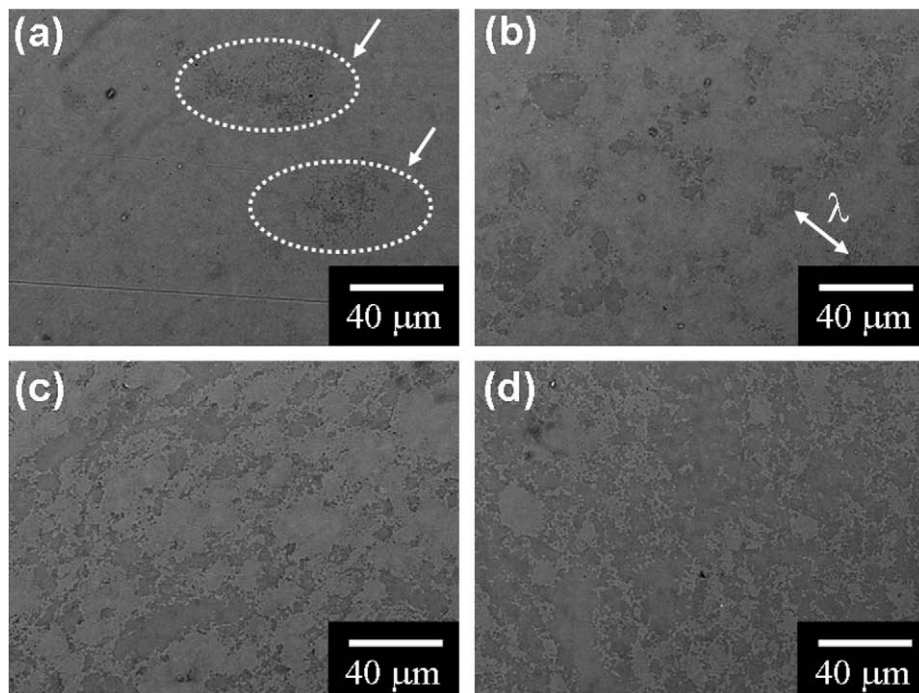


Fig. 2. SEM micrographs for the consolidated composites with: (a) 20 vol.%, (b) 40 vol.%, (c) 60 vol.% and (d) 80 vol.% of β -Al $_3$ Mg $_2$ reinforcement.

ever, the composites show a remarkably reduced plastic deformation of about 1–2% (Table 1). Nevertheless, it was possible to evaluate a 0.2% offset yield strength for these samples.

A high specific strength (tensile or compressive strength divided by the density) is one of the most important aspects of lightweight materials. In the current composites containing high volume fractions of reinforcement, the β -Al₃Mg₂

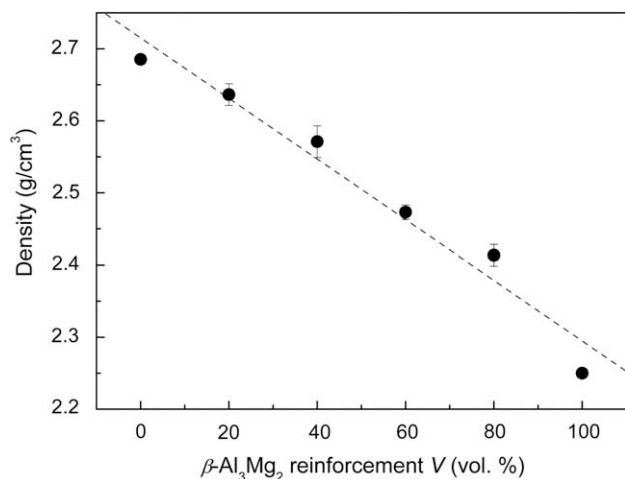


Fig. 3. Density of the consolidated samples as a function of the volume fraction of β -Al₃Mg₂ reinforcement.

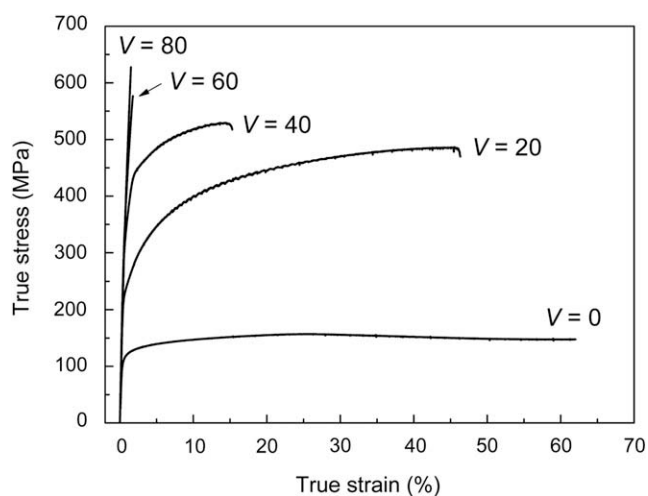


Fig. 4. Room temperature compression true stress–true strain curves for the hot pressed and hot extruded pure Al ($V=0$), composites with 20 vol.% ($V=20$), 40 vol.% ($V=40$), 60 vol.% ($V=60$) and 80 vol.% ($V=80$) of β -Al₃Mg₂ particles.

Table 1
Experimental data of yield strength (σ_y) and strain at break (ϵ_f).

V (vol.%)	σ_y (MPa)	ϵ_f (%)
20	227 ± 10	46.0 ± 3.5
40	342 ± 15	15.0 ± 1.1
60	448 ± 20	2.0 ± 0.2
80	589 ± 20	1.5 ± 0.3

leads to a remarkable strengthening contribution to the mechanical properties of the Al matrix. Moreover, the addition of low-density β -Al₃Mg₂ particles decreases the density of the composites below that of pure Al (Fig. 3). The increase of strength together with the simultaneous decrease of density remarkably increases the specific strength of the current composites, as shown in Fig. 5. The specific strength sharply increases from about 55 kN m kg⁻¹ for pure Al to 180 kN m kg⁻¹ for the composite with 20 vol.% of β -Al₃Mg₂. The specific strength further increases with increasing volume fraction of reinforcement up to about 250 kN m kg⁻¹ for the composite with $V=80$. These values of specific strength are higher than those reported for Al/SiC_p [34] and Al/Al₂O₃ [35] composites evaluated by compression or bending tests (Fig. 5), which indicates that composites reinforced with CMA particles may be a valid alternative to conventional ceramic-reinforced composites.

3.2. Modeling of mechanical properties

The experimental values of the room temperature yield strength of the composites are presented in Table 1 and the normalized yield strength (normalized to the yield strength of pure aluminum, $\sigma_y^0 = 113$ MPa) is shown in Fig. 6 (data points) as a function of the reinforcement content. The yield strength is very sensitive to the volume fraction of reinforcement and rises significantly with increasing V . For example, the yield strength for the composite with $V=20$ is 227 MPa, which is two times higher than the unreinforced Al matrix. The yield strength of the composites further increases with increasing amount of reinforcement reaching a value of 589 MPa for the sample with $V=80$ (five times higher than that for the unreinforced material).

The strengthening effect of particles in metal matrix composites can be mainly attributed to two factors [36]:

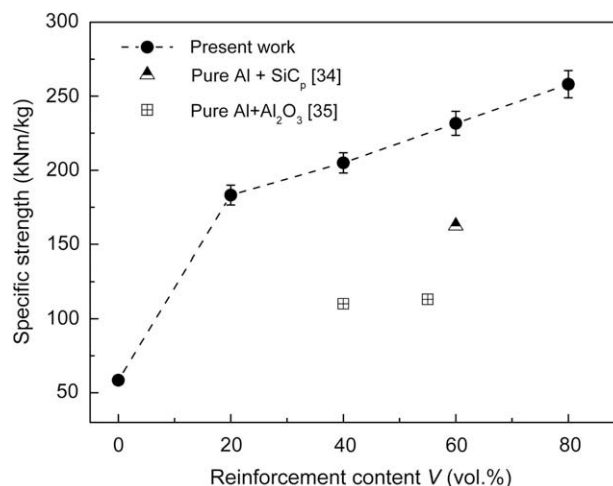


Fig. 5. Specific strength of the composites as a function of the amount of CMA reinforcement. For comparison purposes, the values for Al-based MMCs reinforced with SiC_p [34] and Al₂O₃ [35] evaluated by compression or bending tests are also reported.

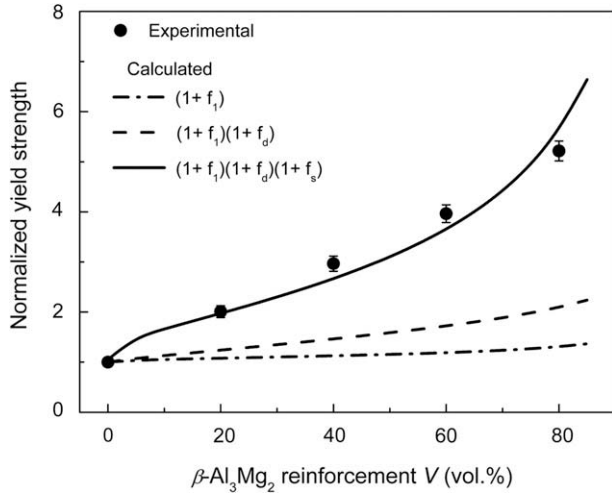


Fig. 6. Normalized yield strength of the consolidated samples as a function of the volume fraction of reinforcement: experimental data (points) and calculated values (lines) from f_1 (load-bearing effect), f_d (dislocation strengthening) and f_s (matrix ligament size).

(i) the load-bearing effect of the reinforcement, in which the reinforcement can share the applied stress directly by stress transfer from the matrix [37–39], and (ii) the dislocation strengthening in the matrix, which is related to the nucleation of additional dislocations in the matrix due to the introduction of the reinforcement [40,41]. These two factors are interdependent and act simultaneously, resulting in a combined effect. Few attempts [42–44] have been made to quantitatively evaluate the combined effect of both the load bearing and the dislocation strengthening. Among these, Ramakrishnan [44] have proposed an expression to incorporate the two factors as

$$\sigma_y = \sigma_y^0(1 + f_1)(1 + f_d), \quad (1)$$

where σ_y^0 is the yield strength of the unreinforced matrix, f_1 is a reinforcing factor related to the load-bearing effect and f_d is the reinforcing factor related to the dislocation strengthening. For particulate-reinforced composites the general expression for f_1 is [38,45]

$$f_1 = 0.5V. \quad (2)$$

f_d is given by

$$f_d = \Delta\sigma_{dis}/\sigma_y^0 \quad (3)$$

where $\Delta\sigma_{dis}$ is the increase of the yield strength caused by dislocation strengthening as [46]

$$\Delta\sigma_{dis} = \sqrt{(\Delta\sigma_{or})^2 + (\Delta\sigma_{the})^2 + (\Delta\sigma_{geo})^2} \quad (4)$$

where $\Delta\sigma_{or}$ is the Orowan stress or the stress increase needed to pass a dislocation through an array of impeding particles, $\Delta\sigma_{the}$ is the stress contribution due to the statistically stored dislocation introduced by the thermal expansion mismatch between matrix and second phase particles and $\Delta\sigma_{geo}$ is the stress contribution due to the strain gradient effects associated with the geometrically necessary dis-

tributions of dislocations required to accommodate the plastic deformation mismatch between the matrix and particles. The analytical expressions for $\Delta\sigma_{or}$, $\Delta\sigma_{the}$ and $\Delta\sigma_{geo}$, which are related to both the volume fraction and the size of the reinforcements, can be found in Refs. [14,47–51].

The yield strength of the current MMCs was calculated using Eqs. (1)–(4) and the parameters used in the calculations are summarized in Table 2. The calculated values of the yield strength are shown in Fig. 6 as a dashed line. The results reveal that Eq. (1) remarkably underestimates the experimental values of the yield strength (data points in Fig. 6) in particular for the composites with high volume fractions of reinforcement. Therefore, this indicates that calculations based on the combined effect of load bearing and dislocation strengthening cannot accurately explain the strengthening effect of the present particulate-reinforced composites. As a result, another strengthening mechanism should be active in the current composites.

The use of large volume fractions of reinforcement and the corresponding microstructure may explain this aspect. As shown in Fig. 2, the Al matrix is partitioned by the reinforcing particles into discrete regions. The size of such regions, i.e. the matrix ligament size λ (see Fig. 2b) decreases with increasing volume fraction and is reduced to few micrometers in the composite with $V = 80$ (Fig. 2d). This size effect, similar to the strengthening by grain refinement, can significantly contribute to the strength of the material because the matrix/particle interface can effectively inhibit dislocation movement [55]. Similarly to the well-known Hall–Petch relationship [56], the strength increase ($\Delta\sigma_s$) caused by the decrease of the matrix ligament size can be expressed as

$$\Delta\sigma_s = k/\sqrt{\lambda} \quad (5)$$

where k is a strengthening constant. The variation of the matrix ligament size as a strengthening effect can be taken into account in the calculations by modifying Eq. (1) as

$$\sigma_y = \sigma_y^0(1 + f_1)(1 + f_d)(1 + f_s), \quad (6)$$

where f_s is the factor related to the matrix ligament size effect and it is given by

$$f_s = \Delta\sigma_s/\sigma_y^0. \quad (7)$$

As a guideline to the experimental measurements of λ , it is simply assumed that the reinforcing particulates are aligned cubes distributed in a simple cubic arrangement,

Table 2
Parameters used in the calculations.

Parameter (unit)	Value	Refs.
E^m (GPa)	71 ± 1	[52]
ν^m	0.33	[51]
E^p (GPa)	49.8	[21]
ν^p	0.27	[21]
μ^m (GPa)	28.0	[53,54]
M	3.1	[53,54]

which leads to the following relationship between the matrix ligament size λ , the volume fraction V (in vol.%) and the diameter of the particles D [57]:

$$\lambda = D \left[\frac{1}{(V/100)^{1/3}} - 1 \right]. \quad (8)$$

The prediction of λ by using Eq. (8) is in good agreement with the experimental results, as shown in Fig. 7a. In addition, Fig. 7a reveals that, besides on the volume fraction V , the matrix ligament size λ strongly depends on the particle size of the reinforcement D . Fine reinforcing particles (10–20 μm) will result in a small matrix ligament size ($\lambda < 25 \mu\text{m}$) for all volume fractions. On the other hand, larger particles ($D > 20 \mu\text{m}$) have a stronger effect on λ , which span over a wider range of values, even exceeding 60 μm . In the present work, the average particulate size is about 40 μm and the volume fraction of reinforcement is

between 20 and 80 vol.%, which are responsible for the observed significant size effect. Fig. 7b shows the correlation between the predicted λ and the experimental values (measured as explained in Section 2). The correlation is linear, which indicates that the matrix ligament size can be adequately described by Eq. (8). For comparison purpose, experimental measurements of λ for Al-based composites reinforced with Al_2O_3 and B_4C prepared by infiltrating method [58] are also shown in Fig. 7b, revealing a strong deviation from linearity of experimental and predicted values for $\lambda > 20 \mu\text{m}$.

The values of the yield strength calculated using Eqs. (6)–(8) with $k \sim 380 \text{ MPa } \mu\text{m}^{1/2}$ (calibrated from fitting) are shown in Fig. 6 (solid line). The calculations are in good agreement with the experimental results. This indicates that the modified strengthening expression (Eq. (6)), which considers the combined effect of load bearing, dislocation strengthening and matrix ligament size, can be used to accurately model the yield strength of composites with high volume fraction of reinforcement. It is worth noticing that the value of k used for the present calculations ($380 \text{ MPa } \mu\text{m}^{1/2}$) is of the same order of magnitude as those for Al–Mg alloys ($k = 260 \text{ MPa } \mu\text{m}^{1/2}$) determined using the Hall–Petch relationship [59]. This suggests that the reduction of matrix ligament size results in a similar strengthening effect as that observed for grain refinement. However, the matrix ligament size effect is a result of the piling up of dislocations at the matrix/particle interface, while the strengthening effect of grain refinement is due to dislocation piling-up at the grain boundaries [55].

This behavior is schematically shown in Fig. 8a. In general, an array of N dislocations (i.e. a dislocation pile-up) will form when the dislocations encounter an obstacle [55]. At the equilibrium, the net force on each of the N dislocations is zero. For edge dislocations, the local stress at the leading dislocation in a pile-up (consisting of the

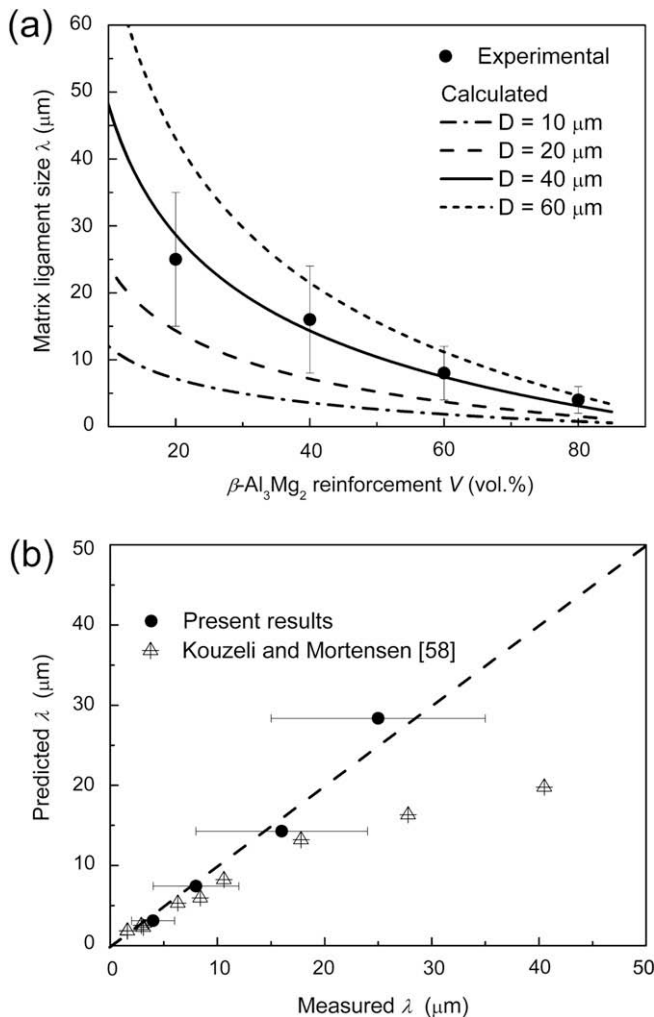


Fig. 7. (a) Experimental data (points) and calculated values (lines) of the matrix ligament size λ as a function of the reinforcement content. (b) Correlation between the predicted and the experimental values of λ . Experimental measurements of λ for Al-based composites reinforced with Al_2O_3 and B_4C prepared by infiltrating method [58] are also shown for comparison.

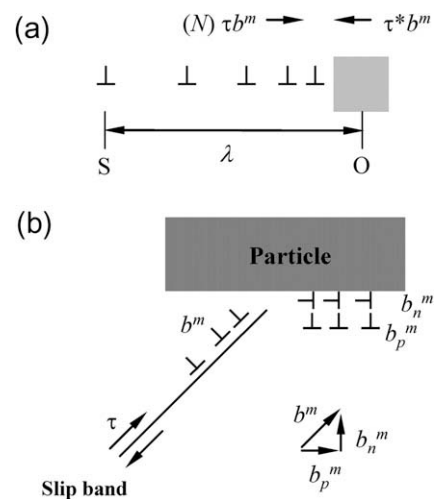


Fig. 8. (a) Schematic illustration of a dislocation pile-up moving from the source S to the obstacle O (e.g. grain boundaries) and (b) schematic illustration showing the deformation of the matrix ligament accommodated by crystal slip parallel to the particle/matrix.

applied stress and the sum of the stress fields of all the other dislocations) is $N\tau b^m$, where τ is the applied stress and b^m is the Burgers vector of the metal. In addition, the leading dislocation encounters the short-range stress field τ^* of the obstacle (e.g. grain boundaries or second-phase particles), which gives rise to a repulsive force $\tau^* b^m$ [55]. At the equilibrium, the two stresses are balanced as

$$N\tau b^m - \tau^* b^m = 0, \quad \text{or} \quad N\tau = \tau^* \quad (9)$$

Similar equilibrium equations can be used for the following dislocations in the pile-up. An analytical integral solution has been proposed to solve these equations, giving the number of dislocations in the pile-up [60,61] as

$$N = \pi(1 - \nu^m)l\tau/\mu^m b^m \quad (10)$$

where ν^m and μ^m are Poisson's ratio and shear modulus of the metal, and l is the length of the pile-up zone. Combining Eqs. (9) and (10) gives the critical stress τ_c required to propagate a dislocation through an obstacle

$$\tau_c = \sqrt{\frac{\mu^m b^m \tau^*}{\pi(1 - \nu^m)l}} \quad (11)$$

τ_c is a material constant, which depends on interface energy and dislocation source [55]. The above expression shows that the applied stress at yield varies with $l^{-1/2}$. With the grain boundaries as barriers, the critical stress τ_c is that required for the dislocations to pass through the grain boundaries. In this case, the largest pile-ups have length $l = d/2$ (d : grain size), giving τ (and σ) $\propto d^{-1/2}$, which is the form of the Hall–Petch relationship [56]. On the other hand, with rigid second phase particles as obstacles and with the matrix enclosed by a high volume fraction of particles, the dislocation pile-ups do not easily pass through the matrix/particle interface to propagate into the adjacent particles. As a result, the yield of the matrix or the deformation of the matrix ligament may be accommodated by crystal slip parallel to the interface, as schematically shown in Fig. 8b. In this case, Eq. (9) can be rewritten as

$$N\tau \cos \theta = \tau^*, \quad (12)$$

where θ is the angle between the slip plane and the particle/matrix interface plane and τ^* can be simply regarded as a critical strength needed to drive the dislocations propagate along the particle/matrix interface. The critical stress can be then related to the matrix ligament size λ by combining Eqs. (10) and (12):

$$\tau_c = \sqrt{\frac{\mu^m b^m \tau^*}{\pi(1 - \nu^m)l \cos \theta}} = \sqrt{\frac{2\mu^m b^m \tau^*}{\pi(1 - \nu^m)\lambda \cos \theta}} \quad (13)$$

where $l = \lambda/2$ and τ_c is now the critical stress needed to drive the dislocation slip parallel to the particle/matrix interface. Without loss of generality, by choosing $\theta = 45^\circ$, Eq. (13) can be rewritten as

$$\tau_c = k'/\sqrt{\lambda}, \quad (14)$$

where k' is a material constant. Similarly to Eq. (5), Eq. (14) is analogous to the classic Hall–Petch relationship and predicts τ (and σ) to be proportional to $\lambda^{-1/2}$. Fig. 9a shows the dependence of the flow stress (0.2% and 0.5% offset) on $\lambda^{-1/2}$. The relationship between flow stress and $\lambda^{-1/2}$ is approximately linear, corroborating the validity of Eq. (13) and demonstrating that the metal ligament size effect plays a dominant role in the strengthening of the composites.

In order to compare the effect of the three reinforcing factors, Fig. 9b and c displays the calculated values of f_s (matrix ligament size), f_l (load-bearing effect) and f_d (dislocation strengthening) as a function of the reinforcement content. The results clearly show that the values of f_s are much larger than both f_l and f_d , which is in agreement with the observation that the dominant strengthening mechanism in the current composites is related to the reduction of the matrix ligament size. In addition, f_l is larger than f_d for all the volume fractions, indicating that the strengthening effect by load bearing is more effective than dislocation strengthening, in particular for reinforcing particles larger than 20 μm .

In order to further verify the validity of the present strengthening model for metal matrix composites containing high volume fraction of reinforcements, experimental data from Kouzeli and Mortensen [58], who have prepared Al-based composites reinforced with 39–58 vol.% μm -sized Al_2O_3 and B_4C particles, have also been analyzed in the framework of the present strengthening model. When the yield strength (0.2% offset) reported by Kouzeli and Mortensen [58] is related to the matrix ligament size λ , a linear relationship between σ_y and $\lambda^{-1/2}$ can be clearly found for both the particle-reinforced composites, as shown in Fig. 10a. The value of k (Eq. (5)), determined from the slopes in Fig. 10a, is about 200 $\text{MPa } \mu\text{m}^{1/2}$ and 250 $\text{MPa } \mu\text{m}^{1/2}$ for the composites reinforced with Al_2O_3 and B_4C particles, respectively. Such a linear relationship is similar to what observed for the composites reinforced with $\beta\text{-Al}_3\text{Mg}_2$ particles (Fig. 9a). Fig. 10b shows the correlation between the predicted (through Eq. (6)) and the experimental values of the yield strength for the composites of Kouzeli and Mortensen [58]. The correlation is linear, which indicates that the present strengthening model based on the matrix ligament size effect can be successfully used to describe the mechanical properties of different types of Al-based metal matrix composites.

The present strengthening model describes remarkably well the mechanical behavior of composites reinforced with large volume fractions (≥ 20 vol.%) of second phase particles. However, it is important to find the lowest volume fraction where this strengthening model can be applied. This aspect can be discussed with micromechanical considerations, as schematically shown in Fig. 11. The present model is based on the assumption that the slip bands in the metal matrix are intensively blocked by the reinforcing particles. In accordance with the model, Fig. 11 shows the particles organized in a cubic arrangement. In such an

arrangement, the most probable path to form unblocked slip bands is parallel to the line AC. Small particle sizes correspond to large values of ligament size, which consequently leads to the easier formation of unblocked slip

bands. At this point, the ligament size effect is negligible. With increasing the particle size and/or decreasing the lig-

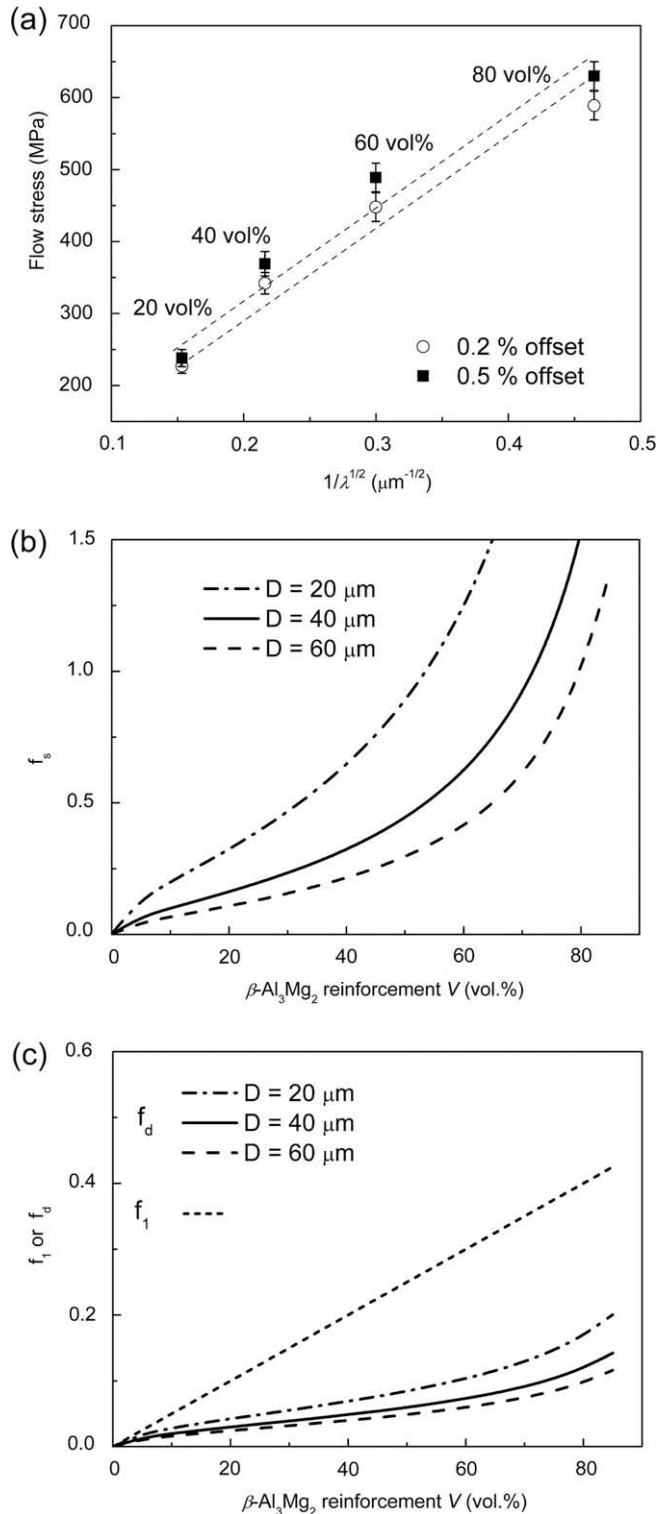


Fig. 9. (a) Dependence of the flow stress (0.2% and 0.5% offset) of the composites on $\lambda^{-1/2}$. Calculated values of (b) f_s (matrix ligament size) and (c) f_1 (load-bearing effect) and f_d (dislocation strengthening) as a function of the volume fraction of $\beta\text{-Al}_3\text{Mg}_2$ reinforcement.

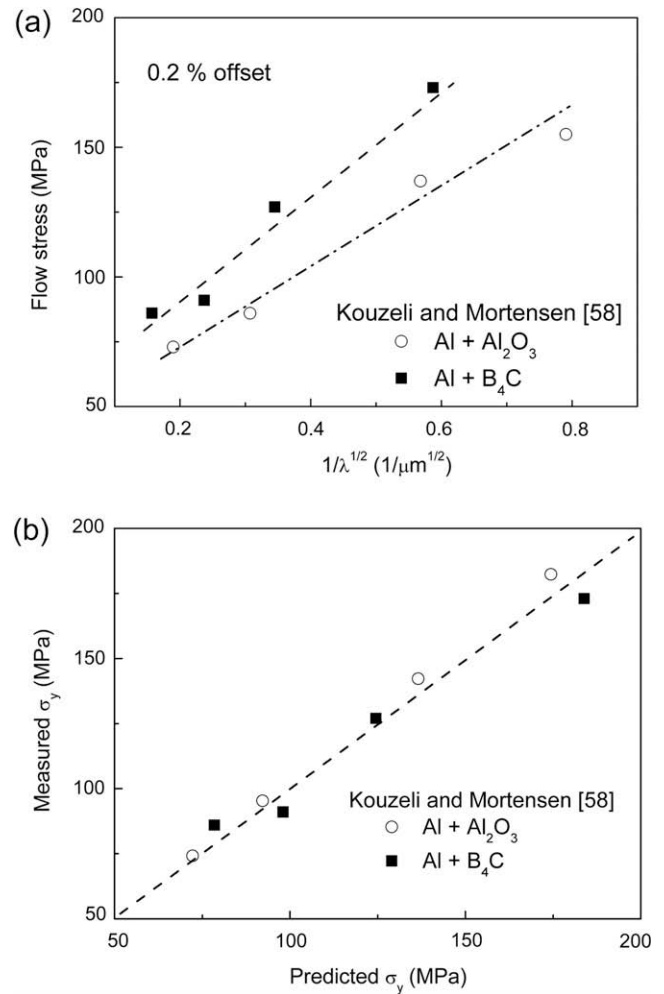


Fig. 10. (a) Dependence of the flow stress (0.2% offset) on $\lambda^{-1/2}$ for Al-based composites reinforced with Al_2O_3 and B_4C particles [58]. (b) Correlation between the predicted (through the present strengthening model) and the experimental values of the yield strength for the composites of Kouzeli and Mortensen [58].

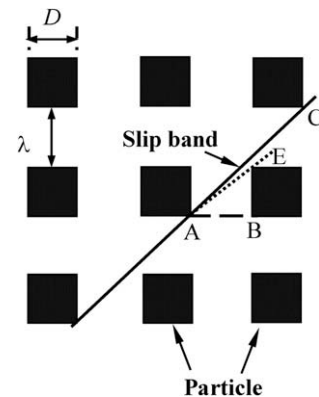


Fig. 11. Schematic illustration of a composite consisting of aligned reinforcing cubic particles distributed in a simple cubic arrangement showing the possible path of the slip bands (see text).

ament size, the slip bands are prone to be blocked by the surrounding particles. From simple geometrical considerations (see Fig. 11) follows that the slip bands will be blocked when the angle $\angle BAE$ is larger than the angle $\angle BAC$, therefore, when

$$\tan(\angle BAE) > \tan(\angle BAC) \quad (15a)$$

or

$$\frac{D}{\lambda} > \frac{D + \lambda}{D + \lambda} = 1 \quad (15b)$$

Combining Eqs. (15b) and (8), the lowest volume fraction where the present strengthening model can be applied was found to be

$$V > 12.5\%. \quad (16)$$

Although this value has been derived for a simple and regular arrangement of particles (cubic particles organized in a cubic arrangement), it nevertheless can be used as a guideline for the application of the present model to composites with more complex particle distributions.

Effective medium approximation (EMA) and related methods have been successfully used to model the elastoplastic deformation of metal matrix composites reinforced with μm -sized second-phase particles [14,62,63]. The EMA-based modeling is also applicable for composites containing high volume fractions of reinforcement [14]. However, the optimized estimation of the yield strength is a necessary prerequisite for any successful modeling of the overall elastoplastic deformation using the EMA iterative calculations. As a typical example, Fig. 12 shows the experimental stress–strain curve for the composite with 40 vol.% of reinforcement (data points) along with the curves calculated using the self-consistent EMA modeling (for details see Ref. [14]). Different values of yield strength (corresponding to the values estimated from Eq. (6)) have been used for the

calculation of the stress–strain curves. The curves obtained using the yield strength evaluated by the load-bearing effect f_1 (dotted line) and by both the load bearing and dislocation strengthening f_1 and f_d (dashed line) underestimate the deformation behavior of the sample. On the other hand, the use of the yield strength estimated by Eq. (6), which considers the combined effect of load bearing, dislocation strengthening and matrix ligament size, leads to a calculated stress–strain curve which is in very good agreement with the experimental results.

4. Conclusions

To test the validity of CMAs as strengthening agents in MMCs, particulate-reinforced Al-based composites consisting of pure Al reinforced with different volume fractions of $\beta\text{-Al}_3\text{Mg}_2$ intermetallic particles have been produced by powder metallurgy methods. Room temperature compression tests reveal that the addition of the $\beta\text{-Al}_3\text{Mg}_2$ reinforcement remarkably improves the mechanical properties of pure Al. In particular, the composites with 20 and 40 vol.% of reinforcement display yield and compressive strengths exceeding that of pure Al by a factor of 2–3, while retaining appreciable plastic deformation ranging between 45% and 15%. The strength of the material is further increased for the samples with 60 and 80 vol.% of $\beta\text{-Al}_3\text{Mg}_2$ phase, however, the composites show negligible plastic deformation. Furthermore, the addition of low-density $\beta\text{-Al}_3\text{Mg}_2$ particles decreases the density of the material below that of pure Al, considerably increasing the specific strength of the composites.

The mechanical properties of the composites have been modeled by taking into account the combined effect of load bearing, dislocation strengthening and matrix ligament size effect. The calculations are in very good agreement with the experimental results and reveal that the reduction of the matrix ligament size, which results in a similar strengthening effect as that observed for grain refinement, is the main strengthening mechanism in the current composites.

Acknowledgments

The authors thank B. Bartusch, M. Frey, H.-J. Klauf and H. Schulze for technical assistance, and U. Kühn and M. Stoica for stimulating discussions. This work was supported by the EU within the frameworks of the European Network of Excellence on Complex Metallic Alloys (NoE CMA) (contract No. NMP3-CT-2005-500140) and by the German Science Foundation under Grant Ec 111/16-2. G. Liu acknowledges the Alexander von Humboldt Foundation for financial support. K.B. Surreddi is grateful for the financial support provided by the DAAD.

References

- [1] Immarigeon GP, Holt RT, Koul AK, Zhao L, Wallace W, Beddoes JC. Mater Charact 1995;35:41.

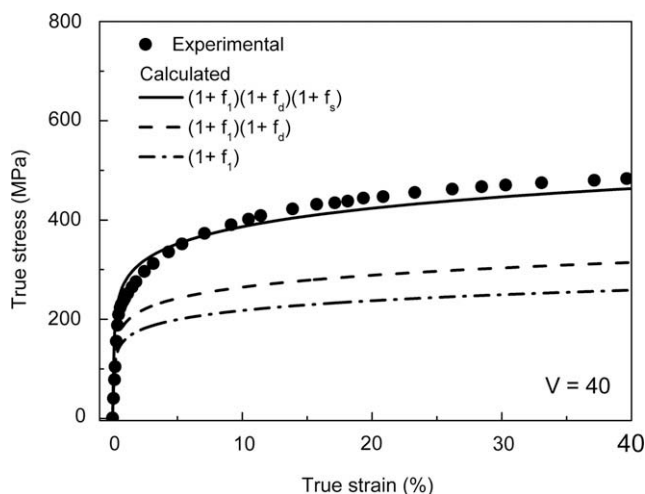


Fig. 12. Room temperature compression stress–strain curve for the consolidated sample with 40 vol.% ($V=40$) of CMA reinforcement: experimental data (points) and calculated values (lines) from f_1 (load-bearing effect), f_d (dislocation strengthening) and f_s (matrix ligament size).

- [2] Cole GS, Sherman AM. *Mater Charact* 1995;35:3.
- [3] Kelkar A, Roth R, Clark J. *JOM* 2001;53:28.
- [4] Clyne TW, Withers PJ. *An introduction to metal matrix composites*. Cambridge: Cambridge University Press; 1993.
- [5] Kainer KU. *Metal matrix composites. Custom-made materials for automotive and aerospace engineering*. Weinheim: WILEY-VCH; 2006.
- [6] Murakami Y. Aluminum-based alloys. In: Cahn RW, Haasen P, Kramer EJ, editors. *Materials Science and Technology*, vol. 8. VCH; 1996. p. 213.
- [7] Miracle DB. *Compos Sci Technol* 2005;65:2526.
- [8] Embury JD, Lloyd DJ, Ramachandran TR. Strengthening mechanisms in aluminum alloys. In: Vasudevan AK, Doherty RD, editors. *Aluminum alloys – contemporary research and applications*, vol. 31. Academic Press, Inc.; 1989. p. 579.
- [9] Slipenyuk A, Kuprin V, Milman Y, Goncharuk V, Eckert J. *Acta Mater* 2006;54:157.
- [10] Tan MJ, Zhang X. *Mater Sci Eng A* 1998;244:80.
- [11] Yu P, Kim KB, Das J, Baier F, Xu W, Eckert J. *Scripta Mater* 2006;54:1445.
- [12] Lee MH, Kim JH, Park JS, Kim JC, Kim WT, Kim DH. *Scripta Mater* 2004;50:1367.
- [13] Scudino S, Surreddi KB, Sager S, Sakaliyska M, Kim JS, Löser W, et al. *J Mater Sci* 2008;43:4518.
- [14] Scudino S, Liu G, Prashanth KG, Bartusch B, Surreddi KB, Murty BS, et al. *Acta Mater* 2009;57:2029.
- [15] Schurack F, Eckert J, Schultz L. *Philos Mag* 2003;83:1287.
- [16] El Kabir T, Joulain A, Gauthier V, Dubois S, Bonneville J, Bertheau D. *J Mater Res* 2008;23:904.
- [17] Tang F, Anderson IE, Biner SB. *Mater Sci Eng A* 2003;363:20.
- [18] Harrigan Jr WC. *Mater Sci Eng A* 1998;244:75.
- [19] Erich DL. *Prog Powder Metall* 1986;46:45.
- [20] Urban K, Feuerbacher M. *J Non-Cryst Solids* 2004;334–335:143.
- [21] Feuerbacher M, Thomas C, Makongo JPA, Hoffmann S, Carrillo-Cabrera W, Cardoso R, et al. *Z Kristallogr* 2007;222:259.
- [22] Dolinšek J, Apih T, Jeglič P, Smiljanić I, Bilušić A, Bihar Ž, et al. *Intermetallics* 2007;15:1367.
- [23] Bauer E, Kaldarar H, Lackner R, Michor H, Steiner W, Scheidt E-W, et al. *Phys Rev B* 2007;76:014528.
- [24] Smontara A, Smiljanić I, Bilušić A, Jagličić Z, Klanjšek M, Roitsch S, et al. *J Alloys Compd* 2007;430:29.
- [25] Maciá E, Dolinšek J. *J Phys: Condens Matter* 2007;19:176212.
- [26] Feuerbacher M, Thomas C, Roitsch S. *Intermetallics* 2008;16:943.
- [27] Demange V, Machizaud F, Dubois JM, Anderegg JW, Thiel PA, Sordelet DJ. *J Alloys Compd* 2002;342:24.
- [28] Roitsch S, Heggen M, Lipińska-Chwałek M, Feuerbacher M. *Intermetallics* 2007;15:833.
- [29] Heggen M, Deng D, Feuerbacher M. *Intermetallics* 2007;15:1425.
- [30] Underwood EE. *Metals handbook*. 9th ed. Metals Park (OH): ASM International; 1985. p. 123.
- [31] ASTM E9-89aR00. *Standard test methods for compression testing of metallic materials at room temperature*. West Conshohocken (PA): ASTM; 2000.
- [32] Scudino S, Sakaliyska M, Surreddi KB, Eckert J. *J Alloys Compd* 2008. doi:10.1016/j.jallcom.2008.07.161.
- [33] ASTM E6-03. *Standard terminology relating to methods of mechanical testing*. Annual book of ASTM standards, vol. 03.01. West Conshohocken (PA): ASTM; 2003.
- [34] Beffort O, Long S, Cayron C, Kuebler J, Buffat PA. *Compos Sci Technol* 2007;67:737.
- [35] San Marchi C, Cao F, Kouzeli M, Mortensen A. *Mater Sci Eng A* 2002;337:202.
- [36] Lloyd DJ. *Int Mater Rev* 1994;39:1.
- [37] Piggot MR. *Load-bearing fiber composites*. Oxford: Pergamon Press; 1980.
- [38] Nardone VC, Prew KM. *Scripta Mater* 1986;20:43.
- [39] Nardone VC. *Scripta Mater* 1987;21:1313.
- [40] Vogelsang M, Arsenault RH, Fisher RM. *Metall Trans A* 1986;17:379.
- [41] Shi N, Wilner B, Arsenault RJ. *Acta Metall Mater* 1992;40:2841.
- [42] Pickard SM, Schmauder S, Zahl DB, Evans AG. *Acta Metall Mater* 1992;40:3113.
- [43] Hirth JP. *Scripta Metall* 1991;25:1.
- [44] Ramakrishnan N. *Acta Mater* 1996;44:69.
- [45] Zhang Q, Chen DL. *Scripta Mater* 2004;51:863.
- [46] Humphreys FJ. In: Anderson SI, Lilholt H, Pedersen OB, editors. *Mechanical and physical behavior of metallic and ceramic composites*. Denmark: Risø Nat Lab; 1988. p. 51.
- [47] Arsenault RJ, Shi N. *Mater Sci Eng* 1986;81:175.
- [48] Miller WS, Humphreys FJ. *Scripta Metall* 1991;25:33.
- [49] Hansen N. *Acta Metall Mater* 1977;25:863.
- [50] Arsenault RJ, Wang L, Feng CR. *Acta Metall Mater* 1991;39:47.
- [51] Brown LM, Stobbs WM. *Philos Mag* 1976;34:351.
- [52] *Metals Handbook. Properties and selection: nonferrous alloys and pure metals*, 9th ed., vol. 2. American Society for Metals; 1979.
- [53] Liu G, Sun J, Nan CW, Chen KH. *Acta Mater* 2005;53:3459.
- [54] Liu G, Zhang GJ, Ding XD, Sun J, Chen KH. *Mater Sci Eng A* 2003;A344:113.
- [55] Hirth JP. Dislocations. In: Cahn RW, Haasen P, editors. *Physical metallurgy*. North-Holland: Amsterdam; 1996. p. 1831.
- [56] Hall EO. *Proc Phys Soc Ser B* 1951;64:747.
- [57] Gustafson TW, Panda PC, Song G, Raj R. *Acta Mater* 1997;45:1633.
- [58] Kouzeli M, Mortensen A. *Acta Mater* 2002;50:39.
- [59] Lloyd DJ, Court SA. *Mater Sci Technol* 2003;19:1349.
- [60] Chou YT, Li JCM. In: Mura T, editor. *Mathematical theory of dislocation*. New York: Am Soc Mech Eng; 1969. p. 116.
- [61] Hirth JP, Lothe J. *Theory of dislocation*. New York: Wiley; 1982.
- [62] Wilkinson DS, Pompe W, Oeschner M. *Prog Mater Sci* 2001;46:379.
- [63] Nan CW, Clarke DR. *Acta Mater* 1996;44:3801.